Mutltifractality of Climate Networks

Adarsh Jojo Thomas[1], Jürgen Kurths[2], and Daniel Schertzer[1,2]

[1]Hydrology Meteorology & Complexity (HM&Co), École nationale des ponts et chaussées, IP Paris, 6-8 Av. Blaise Pascal, Champs-sur-Marne, France
[2]Department of Complexity Science, Potsdam Institute for Climate Impact Research, Telegrafenberg A31, 14473 Potsdam, Germany

Correspondence: Adarsh Jojo Thomas (adarsh-jojo.thomas@enpc.fr)

Abstract.

Geophysical fields are extremely variable over a wide range of space-time scales. More specifically, they are intermittent in the sense that the strongest fluctuations are increasingly concentrated on sparser and sparser fractions of the space-time domain. Multifractals have been developed to analyze and simulate across scales such multiscale intermittency, while climate networks can detect and characterize extreme event synchronisation. In contrast to multifractal analysis, climate networks are usually generated at a given observation scale, despite displaying complex structures over larger scales and likely exhibiting similar complexity at smaller scales.

In this letter, we present how to overcome this dichotomy of approaches by analyzing in detail the effects of increasing the observation scale for climate networks, as allowed by empirical data, i.e. how do they upscale. This must be understood as a preliminary step to be able to downscale them, including for practical applications such as urban geosciences that require analysis and simulation of intermittent fields at very high resolution. This is one of the reasons why we are using precipitation to illustrate our multifractal climate network approach.

1 Introduction

Climate Networks (Tsonis and Roebber, 2004; Donges et al., 2009) have been extensively used to study long-range dependence / synchronization (teleconnection) between different spatial locations of various geophysical fields using different statistical methods such as cross-correlation (Tsonis and Roebber, 2004; Donges et al., 2009), event synchronization (Malik et al., 2012; Boers et al., 2019), mutual information (Hlinka et al., 2013; Donges et al., 2009) to name a few. However, geophysical processes are highly intermittent and varying in intensity, emerging from complex nonlinear interactions across different space-time scales. Networks are typically constructed at the available data resolution and do not account for possible inter-/intra-scale interactions. Recent advances in this direction have combined a wavelet-based approach to tentatively account for synchronizations at different temporal scales (Agarwal et al., 2017; Kurths et al., 2019).

In contrast, multifractals (Schertzer and Lovejoy, 1987; Schertzer et al., 1997; Schertzer and Lovejoy, 1991; Lovejoy et al., 2010) provide a natural framework to analyze and simulate extremely varying and intermittent geophysical and environmental fields over various scales. The core idea is to regard these complex systems as a cascade of structures (Richardson, 1922; Ya-

glom, 1966; Mandelbrot, 1974) across a wide range of scales, thus generating long-range nonlinear interactions between them. We here propose a substantial extension of the climate network approach to multiple scales in a systematic way, accounting for the intermittency and anisotropy in space-time highlighted by multifractals, which is able to capture dynamical behaviors of long-range interactions.

2 Data and Methods

Although our multifractal climate network approach is quite general, we will introduce it and illustrate it with the Tropical Rainfall Measuring Mission (TRMM) satellite and gauge combined gridded precipitation dataset 3B42-v7 (Huffman et al., 2007, 2016). Specifically, a subset of the dataset over the South Asian subcontinent (3.875°-38.875° N, 63.125°-97.125° E) is used to analyze the extensively researched Indian Summer Monsoon (ISM), which is large enough to include some range of teleconnections while remaining computationally feasible. Data were sampled from June to September (122 days), typically associated with monsoon activity, from the total available time period of 22 years (1998-2019). The selected dataset has a high spatial resolution of $0.25° \times 0.25°$ (roughly 20,000 grid points), and daily aggregates of 3-hour high-resolution data are used to avoid the effects of synchonization / dependence induced by the diurnal cycle on networks.

2.1 Multifractal Analysis of Precipitation

Cascades and multifractals originate from turbulence and physically correspond to the concentration of the turbulent energy flux along the cascade to smaller and smaller fractions of the embedding space-time space. The large multiplicity of interactions can generate universal properties, which are defined by only a few relevant parameters that are further physically meaningful (Schertzer and Lovejoy, 1987; Schertzer et al., 1997). The resulting Universal Multifractal (UM) framework has often been used to analyze the precipitation component of the weather and climate (Lovejoy and Schertzer, 2013). In order to analyze the rain rate R, the data is systematically coarse-grained in space and/or time to decrease its resolution. Let L denote the largest scale and ℓ denote the degraded resolution, then the scale-ratio $\lambda = L/\ell$ is the (dimensionless) resolution. The scale-ratios in space and time can be respectively denoted separately by λ_s and λ_t when both are degraded to different resolutions. They are related by $\lambda_t \approx {\lambda_s}^{2/3}$ to account for the anisotropy between horizontal space and time (Schertzer and Lovejoy, 1987, 1989, 1991) and is typically applied to 2D+1 space-time fields.

Let φ_λ be the underlying cascading field conserved at all scales, i.e $\langle \varphi_\lambda \rangle = \text{constant}$. Then the scaling parameter H characterizes the deviation of the rain rate R_λ (at resolution λ) from conservation:

$$\Delta R_\lambda \approx \varphi_\lambda \lambda^{-H} \implies \langle |\Delta R_\lambda| \rangle \approx \lambda^{-H} \,. \tag{1}$$

where the sign $\approx$ means an asymptotic equivalence for large resolutions ($\lambda \gg 1$), i.e. with prefactors $\neq 1$ and possibly coupled with an equality in the probability distribution when random variables are involved. The normalized moments of φ_λ scale with the moment scaling exponent $K(q)$:

$$\frac{\langle \varphi_\lambda^q \rangle}{\langle \varphi_1 \rangle^q} = \lambda^{K(q)} \,. \tag{2}$$

Similarly the exceedance probability distribution of φ_λ scales with the codimension function $c(\gamma)$:

$$\Pr\left(\frac{\varphi_\lambda}{\langle\varphi_\lambda\rangle} \geq \lambda^\gamma\right) \approx \lambda^{-c(\gamma)}, \tag{3}$$

where $\gamma = \log(\varphi_\lambda/\langle\varphi_\lambda\rangle)/\log\lambda$ is the scale-invariant singularity. Both the moment and probability exponent functions are related by the following Legendre transforms (Parisi and Frisch, 1985):

$$K(q) = \max_\gamma(q\gamma - c(\gamma)), \quad c(\gamma) = \max_q(q\gamma - K(q)). \tag{4}$$

Under the UM framework, both $K(q)$ and $c(\gamma)$ of conservative multifractal fields depend only on the parameters α, C_1 :

$$K(q) = \begin{cases} \frac{C_1}{\alpha-1}(q^\alpha - q), & \alpha \neq 1 \\ C_1\, q\log(q), & \alpha = 1 \end{cases} \tag{5}$$

$$c(\gamma) = \begin{cases} C_1\left(\frac{\gamma}{C_1\alpha'} + \frac{1}{\alpha}\right)^{\alpha'}, & \alpha \neq 1 \quad (\text{with } 1/\alpha + 1/\alpha' = 1) \\ C_1\exp\left(\frac{\gamma}{C_1} - 1\right), & \alpha = 1 \end{cases} \tag{6}$$

where $0 \leq \alpha \leq 2$ measures the degree of multifractality, with $\alpha = 0$ for monofractal fields and $\alpha > 1$ for the class of multifractal processes having unbound extreme singularities, and $0 \leq C_1 \leq d$ is the codimension of the mean field (d is the dimension of the embedding space). Figure 1 plots the estimated $K(q)$ curve using single trace moments (TM) (Schertzer and Lovejoy, 1987; Lavallée et al., 1992) of the conserved field at different scales in space and time (see Eq. (2)). Equation (5) then yields the values of α, C_1 from $K(q)$. H can be estimated similarly using the first-order structure function (see Eq. (1)), and also from the relation $\beta = 2H + 1 - K(2)$ between the spectral scaling exponent β and the second-order moment exponent $K(2)$ as shown in Fig. 1.

2.2 Precipitation Climate Networks using Time-Delayed Mutual Information

Climate Networks are constructed between time series R_i, R_j at different geographical locations called nodes or vertices $i, j \in V$ by connecting pairs of them with links (denoted $i \sim j$) if a given measure of similarity $S(R_i, R_j) \geq 0$ of the pair is significant. Unweighted CNs can be constructed from the strongest similarities by thresholding the similarity matrix S :

$$A_{i,j} = \Theta(S_{i,j} - \theta) - \delta_{i,j} = \begin{cases} 1, & S_{i,j} \geq \theta,\ i \neq j \\ 0, & \text{otherwise} \end{cases}, \tag{7}$$

where A is used to denote the adjacency matrix of a network, θ is some threshold on S, $\delta(x)$ is the Kronecker delta to remove self links $i \sim i$ and $\Theta(x)$ is the Heaviside function. The links of a network can be directed, possibly implying a direction of causality between two connected time series. However, we will be focusing on undirected networks here and consequently to symmetric similarity and adjacency matrices. Network centrality measures like the degree ($\deg_i = \sum_j A_{i,j}$) , which gives the number of links connecting a given node, are used to study a network's properties.

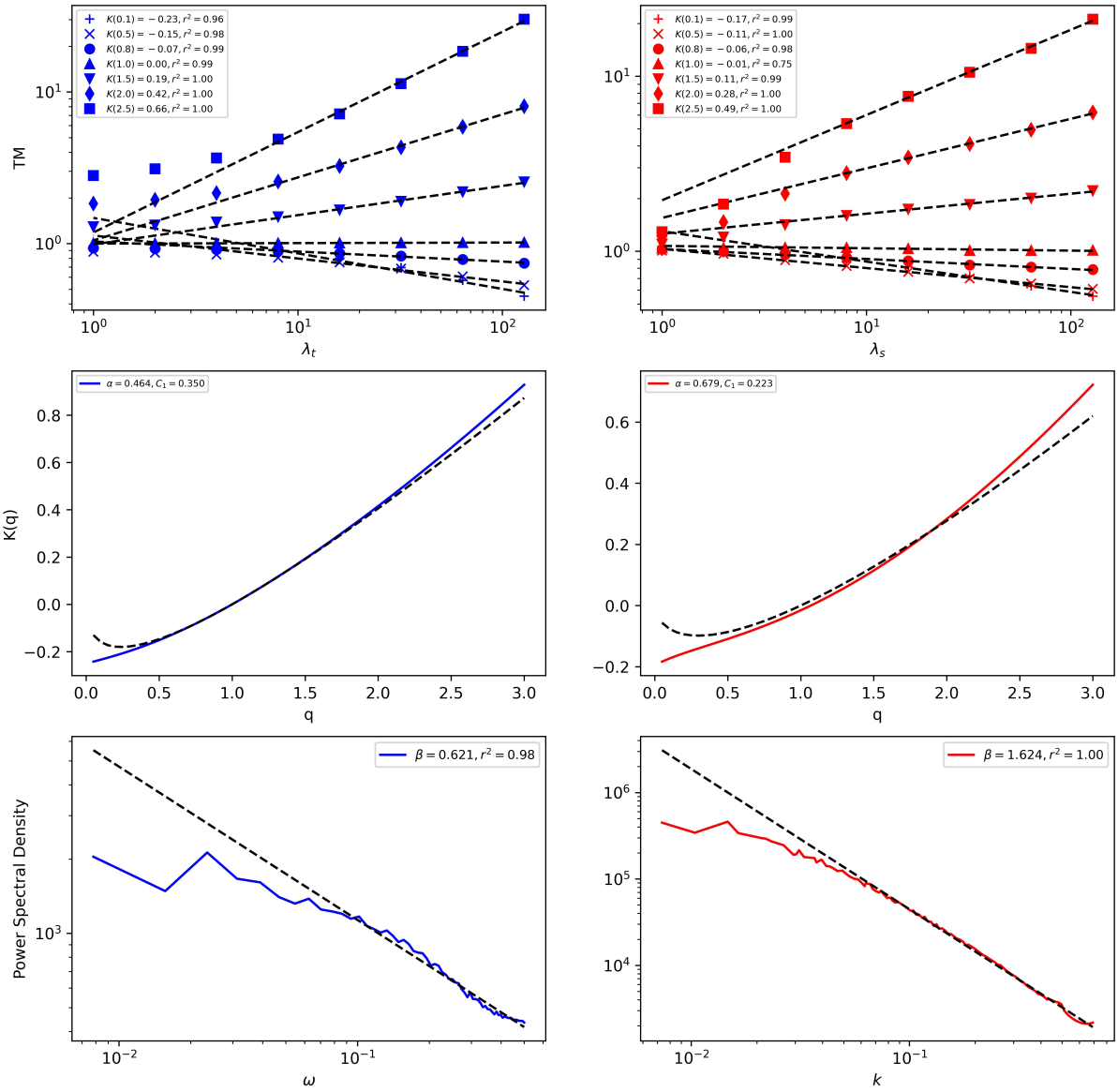

Figure 1. A set of graphs computing the UM parameters for time and space in the left and right columns respectively. Trace Moment (TM) plots are shown in the first row, with scale-break at 440 km in space and 16 days in time. The second row plots the moment scaling exponent $K(q)$ obtained from the TM in the first row. Parameters α, C_1 calculated from $K(q)$ are also shown, along with the corresponding theoretical $K(q)$ curves (dotted line). Power spectra shown in the third row, which was used to estimate H from the spectral slope β, also indicates the deviation in scaling around 460 km in space and 10 days in time. The break around 16 days can be attributed to the synoptic maximum in time. Whereas, the break around 440-460 km is difficult to explain but could be attributed to the spatial scale for synoptic Indian Summer Monsoon (ISM) activity (estimated in (Malik et al., 2012)), since it disappears when samples from the whole year are analyzed.

Time-Delayed Mutual Information (TDMI) (Hlaváčková-Schindler et al., 2007; Hlinka et al., 2013; Haas et al., 2023) has been used here to estimate the general dependence between two time series. Let $R_\lambda(\boldsymbol{x},t)$ denote precipitation time series at the position vector $\boldsymbol{x}$, time t and resolution λ; then TDMI is calculated as follows:

$$I\left(R_\lambda(\boldsymbol{x},t),R_\lambda(\boldsymbol{y},t+\tau)\right)=\iint p\left(R_\lambda(\boldsymbol{x},t),R_\lambda(\boldsymbol{y},t+\tau)\right)\log\left(\frac{p\left(R_\lambda(\boldsymbol{x},t),R_\lambda(\boldsymbol{y},t+\tau)\right)}{p\left(R_\lambda(\boldsymbol{x},t)\right)p\left(R_\lambda(\boldsymbol{y},t+\tau)\right)}\right)dR_\lambda(\boldsymbol{x},t)\,dR_\lambda(\boldsymbol{y},t+\tau), \quad (8)$$

where $p\left(R_\lambda(\boldsymbol{x},t)\right), p\left(R_\lambda(\boldsymbol{x},t)\,R_\lambda(\boldsymbol{y},t+\tau)\right)$ are the marginal and joint distributions respectively. TDMI can also be used by thresholding the rain to account for dependence between extreme rain events. The TDMI based similarities between two time series $R_\lambda(\boldsymbol{x},t),R_\lambda(\boldsymbol{y},t+\tau)$ is then given by:

$$S_\lambda(\boldsymbol{x},\boldsymbol{y})=\frac{I_\lambda(\boldsymbol{x},\boldsymbol{y})}{\max\left(I_\lambda(\boldsymbol{x},\boldsymbol{x}),\,I_\lambda(\boldsymbol{y},\boldsymbol{y})\right)},\ \text{where}\ I_\lambda(\boldsymbol{x},\boldsymbol{y})=\max_{\delta(\boldsymbol{x},\boldsymbol{y})<\tau\leq\tau_\lambda} I\left(R_\lambda(\boldsymbol{x},t),R_\lambda(\boldsymbol{y},t+\tau)\right). \quad (9)$$

The delay at which the dependence is maximized between two time series is called the correlation delay $\tau(\boldsymbol{x},\boldsymbol{y})$ as a function of the position vectors. A maximal delay τ_λ is set while computing the similarity between any two pairs of time series, to limit the creation of false links from unreasonably large $\tau(\boldsymbol{x},\boldsymbol{y})$. The denominator proposed above acts as a normalizing factor which accounts for the self-information (auto-correlation) between time series. More detailed information on the TDMI properties and its implementation can be found in the supplementary.

3 Climate Networks at Multiple Scales

3.1 Coarse Field Networks (CFN)

As pointed out in the introduction, the change of scale for CNs can have at least two meanings:

i) It can correspond to coarse graining of the rainfall data in space-time using the scale ratios from Sect. 2.1 and obtain networks at various larger scales, calculated here for up to 5 different scales in this letter (see Table 1).

ii) This can also be done the other way around, i.e., computing the climate network at a given scale and then degrading its resolution.

Multifractal Climate Networks (MCN) will be used to denote both these definitions. In this subsection, we proceed with the first definition of MCN, called Coarse Field Networks (CFN). They are constructed over a range of scales where the UM parameters remain unchanged (upto the scale break in Fig. 1), and are parameterised by p_λ,θ_λ and τ_λ which depend on the data resolution λ.

TDMI-based CFN are constructed here for two case scenarios: (A) Using similarity measure from the whole range of precipitation values, and (B) from extreme precipitation events above a certain threshold rainfall value, in fact a fixed singularity γ. The threshold rain value required for (B) can be calculated from the multifractal relation in Eq. (3) :

$$p_\lambda=\Pr\left(R_\lambda\geq\lambda^\gamma\right)\approx\lambda^{-c(\gamma)}. \quad (10)$$

Table 1. MCN parameter values used for the computing CNs at 5 different scales are shown below. The p_λ values for case A are omitted from this table since it equates to taking the complete range of rainfall values for each scale. Length scale values in column two correspond to grid lengths at the equator.

Time-scale (days)	Length-scale (km)	Case B : $p_\lambda\,(\%)$	Max lag τ_λ (time-step)	Link-density $\rho_\lambda\,(\%)$
1	27.75	15	20	5
2	83.25	22	10	10
3	138.75	27	7	14
4	222	31	5	18
5	305.25	35	4	22

The corresponding parameter p_λ, which only applies to (B) since (A) does not require thresholding, was fixed at the largest resolution ($p_\Lambda = 0.15$) and calculated for the rest of the scales using Eq. (10) by keeping constant the singularity γ (see Table 1 for p_λ values).

The adjacency matrix A is obtained by thresholding the similarity matrix S_λ with some threshold parameter θ_λ (see Eq. (7)). This θ_λ directly influences the network structure and its properties like degree, link distribution, clustering coefficient, etc., by controlling the density of links, denoted by ρ_λ. If S_λ is assumed to be a multifractal measure, then an equation similar to Eq. (10) is obtained relating ρ_λ at different scales to the threshold singularity γ_S:

$$\rho_\lambda = \Pr\left(S_\lambda \geq \theta_\lambda\right) = \lambda^{-c_S(\gamma_S)};\ \theta_\lambda = \lambda^{\gamma_S}\,. \tag{11}$$

Finally, the τ_λ free parameter sets the maximal delay (lag) up to which the strength of dependence between two given time series is calculated. This maximal correlation time-scale is usually significantly larger than the average lifetime of rain events at a given resolution, which makes it difficult to estimate at different scales. The Coarse Field Network (CFN) computations for $\tau_\Lambda > 40$ days were found to significantly change the spatial pattern of node degrees, whereas the results remained consistent when varied between 6 and 20 days. Therefore, τ_Λ was fixed to 20 days at scale Λ. For $\lambda < \Lambda$, τ_λ is lowered to keep the effective maximal delay at all scales nearly constant at 20 days, i.e., $\tau_\lambda = \tau_\Lambda \lambda_t^{-1}$ (see Table 1).

3.2 Scaled Climate Networks (SCN)

To analyze the effect of a change of scale on CNs and their properties (e.g., their degrees), we introduce a pair of operators:

- U_λ for upscaling or coarse graining by a scale ratio λ (not always explicitly stated, for the sake of simplicity)
- C for constructing a climate network from a given dataset

They have a more or less immediate meaning when applied to a given field F and we have first considered the composed operator $C \cdot U$ applied to the TRMM rain field (see Sect. 3.1 on CFN). We have also evoked the "other way around", i.e. the

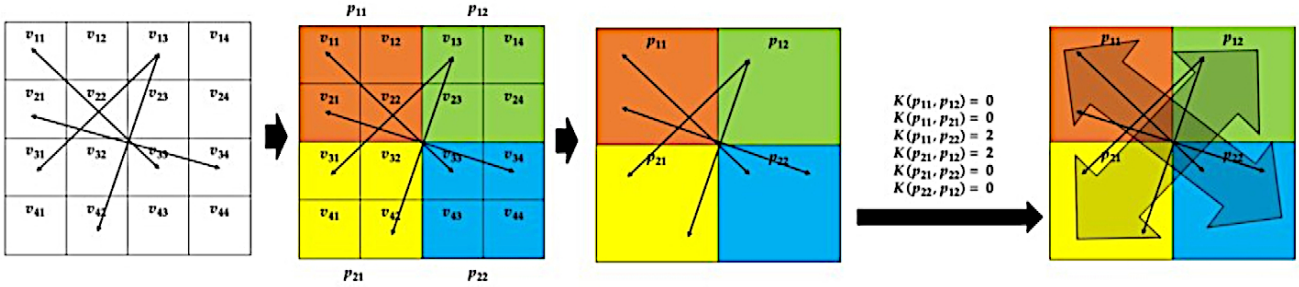

Figure 2. Scaled Climate Network (SCN) schematic : Smaller nodes are grouped together, shown here in different colors, with linked nodes being replaced by linked-groups. The grouping of the node-set directly corresponds to the upscaling of the field in space.

composed operator $U \cdot C$, which will be detailed below as Scaled Climate Networks (SCN), with the difficulty that U needs to be generalised to be applied to a network instead of a field. In fact, U should coarse grain both components of a network, i.e. nodes and links, while fields have only the former component and U is then restricted (and defined) to only act on this unique component.

As an introductory example, we consider the U upscaling operator for unweighted CNs. It seems straightforward to impose the following rather simple rule (Fig. 2 for illustration): two upscaled nodes I and J are linked (i.e. the upscaled adjacency matrix satisfies: $A_{I,J} = 1$) if and only if, they contain more than a given number θ_λ of linked pairs of nodes $\{i, j\}$ belonging respectively to either of the scaled nodes (e.g., $i \in I, j \in J$). A priori, for such Scaled Climate Networks (SCN), this threshold number θ_λ scales with the scale ratio λ of the performed upscaling, similar to Eq. (11). Please note that the physical meaning of θ_λ here does not correspond to its usage in Eq. (11), but was kept only to signify the similar functionality of the parameters as in Eq. (7).

Figure 3 plots the relative degrees (normalized to 0-1 range) computed for the selected scales, by first constructing the network from field F_λ at these different scales, to obtain $CU_\lambda(F_\Lambda)$ described as CFN in Sect. 3.1, and to proceed in the reverse order to obtain $U_\lambda C(F_\Lambda)$ respectively (as SCN). The network operator C acting on F_λ has resolution dependent parameters and the λ notation has been reserved for the parameters alone for the sake of simplicity. Both these approaches are plotted for the two cases (A) and (B) in Sect. 3.1, with CFN and SCN plots in the top and bottom rows respectively. Moving from left to right, the hubs (high-degree nodes) over North Pakistan diminish (have reduced degree) at larger scales and simultaneously new hubs emerge in parts of central India. This further emphasises the need for a multiscale approach to CNs for improved understanding of the climate dynamics at different scales. Differences in the network structures between these two approaches are very noticeable from both the figures even for such a small range of scales. Local structural differences can be tentatively quantified with the Jaccard distance (Donnat and Holmes, 2018) defined below (where $|A|$ denotes the cardinality of the set A):

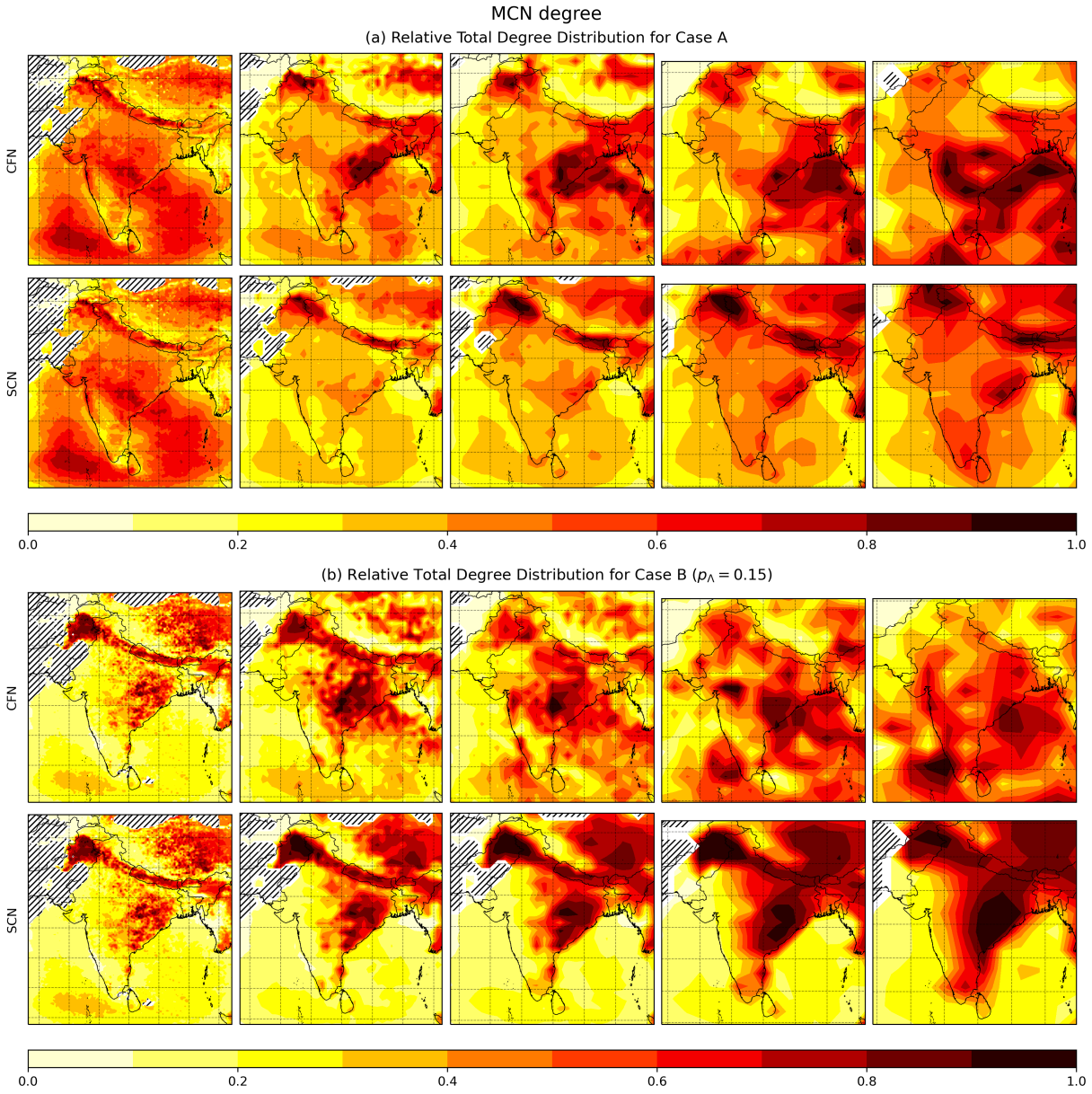

Figure 3. Relative Degrees for both approaches Coarse-Field Networks (CFN, top row) and Scaled Climate Networks (SCN, bottom row) at different scales λ are plotted for two cases (a) Case A : full-range of the rain rate and (b) Case B : $p_\Lambda = 0.15$ thresholded time-series (see table 1 for all parameter values). The resolution in space decreases from left to right. The distribution of CFN hubs (high-degree nodes) in space differ significantly with decreasing resolution compared to the SCN hubs which are more stable and appear to be independent of it (and more prominent in (b)). The dashed regions were not included in the analysis for a lack of samples due to scanty rainfall (<15% rainy days during the period of study).

$$d_{\text{Jac}} = 1 - \frac{\sum([CU_\lambda F_\Lambda \cap U_\lambda C F_\Lambda])}{\sum([CU_\lambda F_\Lambda \cup U_\lambda C F_\Lambda])} = \frac{\sum |[C, U_\lambda] F_\Lambda|}{\sum([CU_\lambda F_\Lambda \cup U_\lambda C F_\Lambda])}\,, \tag{12}$$

which provides the relative number of common links between both ways of upscaling with respect to the total number of links, and is therefore a measure of their similarity. The second equality of Eq. (12) shows that d_{Jac} is also a metric of the relative non-commutativity of the operators C and U_λ.

The Jaccard distance d_{Jac} between the Coarse Field (CFN) and Scaled Climate (SCN) networks is plotted versus the logarithm of the nondimensionalized resolution ℓ_s in Fig. 4 for both cases (A) and (B). It significantly increases with upscaling and corresponding resolution λ_s decrease. The overall increase to $d_{\text{Jac}} \approx 60 - 70\%$ indicates that the local network properties have changed drastically for both cases, although the increase for (A) is significantly lower ($\approx 10\%$) than for (B), i.e. taking into account all the fluctuations, not only the extremes like for (B). The SCN exhibit scale invariance in spatial distribution of the degree in contrast to CFN degree patterns which change with scale. This supports the limited commutativity of the network constructor C with the upscaling operators $U_\lambda C \neq C U_\lambda$ for large upscaling, as already pointed out above.

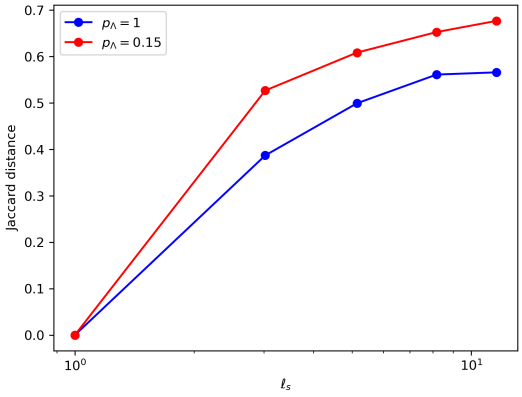

Figure 4. Scale by scale network dissimilarity between Coarse Field (CFN) and Scaled Climate (SCN) networks displayed by the plots of the Jaccard distance $d_{\text{Jac}} \in [0, 1]$ vs. $\log_{10} \ell_s$ (cases A (blue) and B (red)).

4 Conclusions

This letter was devoted to analyzing the multifractality of climate networks, while their scale dependence is too often ignored. This was achieved by first analyzing the space-time multifractal properties of a test field, which was also analyzed in the framework of climate networks. This enabled us to study the upscaling of climate networks. We first highlighted that there is not a single definition of an upscaling of climate networks due to a relative non-commutativity of two elementary operators, namely constructing a network from a given dataset and coarse graining it. This was first shown on the degree of the networks, then we highlight the importance of the Jaccard distance as a theoretical and practical metric of the relative non-commutation.

The above results are fairly general, but the choice of monsoon rainfall data as a test field was motivated by many interests ranging from the social to the scientific. A common major interest is that of huge extremes, which have an overwhelming importance for understanding and modelling the water cycle. Scale-dependent parameters were formulated, allowing for the systematic inference of network structures at larger scales. Our results not only confirm their scale dependence but also a significant sensitivity to the type of scale change, with the identification of new regions of interest emerging at larger scales in the case of coarse-field networks previously undetected in single-scale network studies. We were able to capture the dynamics of processes with the potential inference of precipitation pathways dominating these scales. On the other hand, the scaled climate networks appear static, unable to identify any new regions.

To summarize, we showed the effectiveness and desirability to analyze climate data using a multiscaling approach. This approach could easily be extended to weighted sparse and dense networks. Also, the formalism developed so far is limited to links between nodes at a given scale. Inter-scale links could be beneficial in further understanding cross-scale dynamics, for better simulations of climatic processes whilst preserving their spatial correlations and improved downscaling of networks and fields.

Code availability. The codes for generating the results are made by scripting Python software. All codes and data used in this study can be obtained from the corresponding author upon reasonable request.

Data availability. The TRMM data can be accessed through (Huffman et al., 2016)

Author contributions. AT carried out all the calculations, analyzed the results and drafted the article. JK and DS co-designed and guided this study, facilitating access to the analysis and simulation software, respectively from PIK for climate networks and HM&Co for multifractals. All the authors contributed to the final version of the manuscript. DS provided funding for this project from École nationale des ponts et chaussées.

Competing interests. Some authors are members of the editorial board of journal Nonlinear Processes in Geophysics.

Acknowledgements. We thank the editor for the acceptance of our work, Prof. A. Tsonis for his insightful feedback as a referee, and the anonymous referee for their constructive comments and suggestions, which greatly improved this work. AT is grateful to his correspondents at the Potsdam Institute for Climate Impact Research (PIK) for their assistance with technical and computational aspects of climate networks.

The authors acknowledge financial and computational support from École nationale des ponts et chaussées (ENPC), in particular an ENPC PhD scholarship for a disruptive thesis (AT). AT and DS also acknowledge partial support from the TI(GA) "Building for the Future, Living in the Future" program.

References

Agarwal, A., Marwan, N., Rathinasamy, M., Merz, B., and Kurths, J.: Multi-scale event synchronization analysis for unravelling climate processes: a wavelet-based approach, Nonlin. Processes Geophys., 24, 599–611, https://doi.org/10.5194/npg-24-599-2017, 2017.

Boers, N., Goswami, B., Rheinwalt, A., Bookhagen, B., Hoskins, B., and Kurths, J.: Complex networks reveal global pattern of extreme-rainfall teleconnections, Nature, 566, 373–377, https://doi.org/10.1038/s41586-018-0872-x, 2019.

Donges, J. F., Zou, Y., Marwan, N., and Kurths, J.: Complex networks in climate dynamics, Eur. Phys. J. Spec. Top., 174, 157–179, https://doi.org/10.1140/epjst/e2009-01098-2, 2009.

Donnat, C. and Holmes, S.: Tracking network dynamics: A survey using graph distances, Ann. Appl. Stat., 12, 971–1012, https://doi.org/10.1214/18-AOAS1176, 2018.

Haas, M., Goswami, B., and von Luxburg, U.: Pitfalls of Climate Network Construction—A Statistical Perspective, J. Climate, 36, 3321–3342, https://doi.org/10.1175/JCLI-D-22-0549.1, 2023.

Hlaváčková-Schindler, K., Paluš, M., Vejmelka, M., and Bhattacharya, J.: Causality detection based on information-theoretic approaches in time series analysis, Phys. Rep., 441, 1–46, https://doi.org/10.1016/j.physrep.2006.12.004, 2007.

Hlinka, J., Hartman, D., Vejmelka, M., Runge, J., Marwan, N., Kurths, J., and Paluš, M.: Reliability of Inference of Directed Climate Networks Using Conditional Mutual Information, Entropy, 15, 2023–2045, https://doi.org/10.3390/e15062023, 2013.

Huffman, G. J., Bolvin, D. T., Nelkin, E. J., and Adler, R. F.: TRMM (TMPA) Precipitation L3 1 day 0.25 degree x 0.25 degree V7, Goddard Earth Sciences Data and Information Services Center (GES DISC) [dataset], https://doi.org/10.5067/TRMM/TMPA/DAY/7, 2016.

Huffman, G. J., Bolvin, D. T., Nelkin, E. J., Wolff, D. B., Adler, R. F., Gu, G., Hong, Y., Bowman, K. P., and Stocker, E. F.: The TRMM Multisatellite Precipitation Analysis (TMPA): Quasi-Global, Multiyear, Combined-Sensor Precipitation Estimates at Fine Scales, J. Hydrometeorol., 8, 38–55, https://doi.org/10.1175/JHM560.1, 2007.

Kurths, J., Agarwal, A., Shukla, R., Marwan, N., Rathinasamy, M., Caesar, L., Krishnan, R., and Merz, B.: Unravelling the spatial diversity of Indian precipitation teleconnections via a non-linear multi-scale approach, Nonlinear Process. Geophys., 26, 251–266, https://doi.org/10.5194/npg-26-251-2019, 2019.

Lavallée, D., Lovejoy, S., Schertzer, D., and Schmitt, F.: On the Determination of Universal Multifractal Parameters in Turbulence, in: Topological Aspects of the Dynamics of Fluids and Plasmas, edited by: Moffatt, H. K., Zaslavsky, G. M., Comte, P., and Tabor, M., NATO ASI Series, Springer Netherlands, Dordrecht, 463–478, https://doi.org/10.1007/978-94-017-3550-6_27, 1992.

Lovejoy, S. and Schertzer, D. (Eds.): The Weather and Climate: Emergent Laws and Multifractal Cascades, Cambridge University Press, Cambridge, https://doi.org/10.1017/CBO9781139093811, 2013.

Lovejoy, S., Tuck, A. F., and Schertzer, D.: Horizontal cascade structure of atmospheric fields determined from aircraft data, J. Geophys. Res., 115, https://doi.org/10.1029/2009JD013353, 2010.

Malik, N., Bookhagen, B., Marwan, N., and Kurths, J.: Analysis of spatial and temporal extreme monsoonal rainfall over South Asia using complex networks, Clim. Dyn., 39, 971–987, https://doi.org/10.1007/s00382-011-1156-4, 2012.

Mandelbrot, B. B.: Intermittent turbulence in self-similar cascades: divergence of high moments and dimension of the carrier, J. Fluid Mech., 62, 331–358, https://doi.org/10.1017/S0022112074000711, 1974.

Frisch, U. and Parisi, G.: Fully Developed Turbulence and Intermittency, in: Turbulence and Predictability in Geophysical Fluid Dynamics and Climate Dynamics, edited by: Ghil, M., Benzi, R. and Parisi, G., North-Holland, New York, 84–

88, https://www.researchgate.net/publication/284646749_On_the_singularity_structure_of_fully_developed_turbulence_in_Turbulence_and_predictability_in_geophysical_fluid_dynamics_and_climate_dynamics, 1985.

Richardson, L. F. (Eds.): Weather Prediction by Numerical Process, Cambridge University Press, Cambridge, https://doi.org/10.1017/CBO9780511618291, 1922.

Schertzer, D. and Lovejoy, S.: Physical modeling and analysis of rain and clouds by anisotropic scaling multiplicative processes, J. Geophys. Res., 92, 9693–9714, https://doi.org/10.1029/JD092iD08p09693, 1987.

Schertzer, D. and Lovejoy, S.: Generalised scale invariance and multiplicative processes in the atmosphere, Pure Appl. Geophys., 130, 57–81, https://doi.org/10.1007/BF00877737, 1989.

Schertzer, D. and Lovejoy, S.: Nonlinear Geodynamical Variability: Multiple Singularities, Universality and Observables, in: Non-Linear Variability in Geophysics: Scaling and Fractals, edited by: Schertzer, D. and Lovejoy, S., 41–82, Springer Netherlands, Dordrecht, https://doi.org/10.1007/978-94-009-2147-4_4, 1991.

Schertzer, D., Lovejoy, S., Schmitt, F., Chigirinskaya, Y., and Marsan, D.: Multifractal Cascade Dynamics and Turbulent Intermittency, Fractals, 05, 427–471, https://doi.org/10.1142/S0218348X97000371, 1997.

Tsonis, A. A. and Roebber, P. J., The architecture of the climate network, Phys. A: Stat. Mech. Appl., 333, 497–504, https://doi.org/10.1016/j.physa.2003.10.045, 2004.

Yaglom, A. M.: Fluctuations in energy dissipation as influencing the shape of turbulence characteristics in an inertial interval, Dokl. Akad. Nauk SSSR, 166, 49–52, https://www.mathnet.ru/eng/dan32002, 1966.